

Supercurrent-induced Anomalous Thermal Hall Effect as a New Probe to Superconducting Gap Anisotropy

Xiaodong Hu,¹ Jung Hoon Han,² and Ying Ran¹

¹*Department of Physics, Boston College, Chestnut Hill, Massachusetts 02467, USA*

²*Department of Physics, Sungkyunkwan University, Suwon 16419, Korea*

(Dated: December 1, 2022)

Two-dimensional superconductors have been realized in various atomically thin films, some of which are anticipated to involve unconventional pairing mechanisms, including twisted bilayer graphene. Due to the low dimensionality, experimental probes of the superconductivity in these systems have been limited. In this paper we consider a Josephson junction formed by stacking two atomically thin films, and propose an anomalous thermal Hall effect induced by the Josephson supercurrent, in the absence of an external magnetic field. We find that this effect can be significant, and interestingly, it sharply probes the *in-plane* anisotropy of the superconducting gap function $\Delta_{\mathbf{k}}$, which may be useful in experimental investigations on two-dimensional superconductivity.

Introduction.—The discovery of the correlated insulating phases and superconductivity in twisted bilayer graphene (TBG) [1, 2] has spurred increasing interest to twisted 2D heterostructures. To understand the possible unconventional superconductivity realized in these systems, intensive experimental investigations have been performed. However, due to the low dimensionality, the majority of studies have been on electrical transport experiments and the available probes have been limited.

On the other hand, the thermal transport has been shown as a powerful probe to reveal the low energy physics of elementary excitations. For instance, the longitudinal thermal conductivity κ_{xx} has been used to probe the gapless quasiparticles in nodal superconductors [3–5]. The thermal Hall effect (THE) κ_{xy} , in the presence of a magnetic field, has been used to investigate the mixed state in superconductors where quasiparticles scatter with vortices [6–8]. In addition, quantized κ_{xy} at low temperatures is a characteristic experimental signature for many 2D topological states. For example, recently quantized thermal Hall effect has been reported in fractional quantum Hall states [9], as well as in quantum spin liquid candidate α -RuCl₃ [10].

The gap function $\Delta_{\mathbf{k}}$ in the momentum space, particularly its anisotropy and possible nodal structures, is one of the most important characteristics of a superconductor, carrying information of the underlying pairing mechanism. $\Delta_{\mathbf{k}}$ may be observed in the angle resolved photoemission spectroscopy (ARPES) [11–13], as well as using quasiparticle interference (QPI) imaging in scanning tunneling spectroscopy (STS) [14, 15]. For low temperature superconductors where $\Delta_{\mathbf{k}}$ is small, however, it can be difficult to resolve the gap anisotropy in ARPES experiments due to the apparatus limit. In addition, for twisted heterostructures, in order to resolve the momentum space in a small moiré Brillouin zone (BZ), the QPI imaging may require a formidably large length scale in the real space. A natural question to ask is that whether there exists other probes sensitive to the gap anisotropy, par-

ticularly when $\Delta_{\mathbf{k}}$ is small. In this paper, we address this question and propose a thermal-transport based physical effect directly sensitive to the gap anisotropy.

Precisely speaking, we consider a Josephson junction formed by vertically stacking two (possibly twisted) thin films, which we coin *bilayer-JJ* in this paper. We study the *in-plane* thermal Hall effect induced by a *vertical* Josephson supercurrent in the *absence* of an external magnetic field, which we term supercurrent-induced anomalous thermal Hall effect (SATHE). The setup is shown in Fig. 1. We derive a simple formula for the

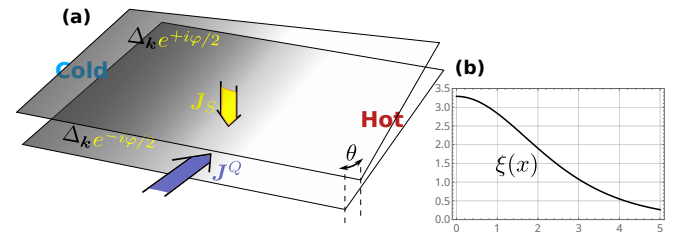


FIG. 1. (a) SATHE for bilayer-JJ. The vertical supercurrent J_S , or a Josephson phase difference φ between the top/bottom layers, would induce an in-plane thermal Hall effect. (b) an illustration for the dimensionless function $\xi(x)$ in Eq.(2).

SATHE, and prove that the signal vanishes identically for an isotropic gap function $\Delta_{\mathbf{k}}$, thus making it possible to use SATHE as a sensitive transport probe of the gap anisotropy. In fact, our result originates from an integral around the Fermi surfaces of topological flavor, as will be shown shortly.

Main results.— Different from the conventional thermal Hall effect, no external magnetic field is present in SATHE and the time-reversal breaking is due to the vertical supercurrent $\propto \sin \varphi$. Recently, the nonlinear Hall effect has been proposed theoretically [16] and observed experimentally [17], where an electrical current induces an electrical Hall effect in metals. SATHE may be viewed as a thermal analogy of the nonlinear Hall effect, and is

a second-order nonlinear response ($\kappa_{xy} \propto \varphi$).

We consider a general bilayer-JJ with a multiband electronic structure. Generically the pairing may occur between different bands $\Delta_{\mathbf{k}}^{a,b} c_{a,\mathbf{k}}^\dagger c_{b,-\mathbf{k}}^\dagger$, where a, b label bands. We firstly study the simple situation where *only the intraband pairing is present* ($\Delta_{\mathbf{k}}^{a,b} = 0$ if $a \neq b$). In addition, in this paper, we assume that $|\Delta_{\mathbf{k}}|$ is much smaller than the energy difference between bands in the normal state. We find that, a small Josephson phase $\delta\varphi$ between the bilayer-JJ induces a change of the Berry curvature, leading to a thermal Hall effect $\delta\kappa_{xy}$:

$$\frac{\delta\kappa_{xy}^{\text{intra.}}}{\delta\varphi \cdot T} = \frac{k_B^2}{16\pi^2\hbar} \sum_{\text{FS}} \text{sign}(v_F) \times \oint_{\text{FS}} dk_{\parallel} \xi \left(\frac{\Delta_{\mathbf{k}}(T)}{k_B T} \right) \cdot \partial_{k_{\parallel}} [\langle u_{\mathbf{k}} | \hat{L} | u_{\mathbf{k}} \rangle], \quad (1)$$

where $\xi(x)$ is the dimensionless function (see Fig.1 (b))

$$\xi(x) \equiv \int_{|x|}^{\infty} dx' \sqrt{x'^2 - x^2} \frac{x'}{1 + \cosh(x')}, \quad (2)$$

$|u_{\mathbf{k}}\rangle$ is the Bloch state of the *normal* state at the Fermi level, and the dimensionless Hermitian operator \hat{L} is the generator of gauge transformation associated with the φ Josephson phase (see Eq.(4) below). The loop integral is performed over each Fermi surface (FS) and k_{\parallel} is the counterclockwise momentum direction tangential to the FS. $\text{sign}(v_F) = \pm 1$ characterizes whether the FS is electron-like or hole-like. (Note that a single band may host multiple FS's.) Clearly if $\Delta_{\mathbf{k}}$ is \mathbf{k} -independent over a FS, the loop integral over that FS becomes one of a total derivative and vanishes identically.

Notice that the SATHE response $\frac{\delta\kappa_{xy}}{\delta\varphi \cdot T}$, apart from the quantum unit $\frac{k_B^2}{\hbar}$, is dimensionless. Because $\varphi = \pi/2$ corresponds to the maximal supercurrent state of a JJ, and noting the $\frac{1}{16\pi^2}$ factor in Eq.(1), we conclude that the size of κ_{xy} in SATHE is generically $\gtrsim 10^{-2}$ of the thermal conductance quantum if the variation of $|\Delta_{\mathbf{k}}|$ around a Fermi surface is significant.

The \hat{L} operator.—In a bilayer-JJ, the normal state tight-binding Hamiltonian can be written in a block form:

$$H_0(\mathbf{k}) = \begin{pmatrix} H_0^t(\mathbf{k}) & T_{\perp}(\mathbf{k}) \\ T_{\perp}^\dagger(\mathbf{k}) & H_0^b(\mathbf{k}) \end{pmatrix}, \quad (3)$$

where t/b labels the top/bottom layer, and T_{\perp} represents the interlayer hopping. In the superconducting state, pairing terms are introduced. Turning on a Josephson phase φ between the two layers is equivalent to performing the following gauge transformation $H_0 \rightarrow UH_0U^\dagger$ while keeping the pairing terms unchanged:

$$U(\varphi) = \begin{pmatrix} e^{-i\varphi/4} & 0 \\ 0 & e^{i\varphi/4} \end{pmatrix} \equiv e^{-i\varphi/4\hat{L}}, \hat{L} = \begin{pmatrix} \mathbf{1} & 0 \\ 0 & -\mathbf{1} \end{pmatrix}. \quad (4)$$

Since $|u_{\mathbf{k}}\rangle$ is the eigenstate of $H_0(\mathbf{k})$, $\langle u_{\mathbf{k}} | \hat{L} | u_{\mathbf{k}} \rangle \in [1, -1]$ is simply the indicator of the layer-component of the state. If T_{\perp} is absent, top/bottom layer decouples and $\langle u_{\mathbf{k}} | \hat{L} | u_{\mathbf{k}} \rangle = \pm 1$, leading to a vanishing SATHE according to Eq.(1), consistent with physical intuitions. The SATHE is mainly contributed by the section of the Fermi surfaces where the interlayer mixing is significant.

Symmetry consideration.— Consistent with the transformation property of κ_{xy} and the Josephson phase φ , in order to have nonzero SATHE, the bilayer-JJ cannot host any mirror plane either perpendicular or parallel to the bilayer plane, but can host either in-plane or out-of-plane rotational axes. In 2D superconductors, it is common that the monolayer system hosts mirror planes. However, any bilayer-JJ formed by twisted layers automatically breaks these mirror planes. Therefore, SATHE is a rather generic physical effect in bilayer-JJ systems.

Derivation of Eq.(1).— Here we briefly discuss the derivation of Eq.(1) and leave the details in [18]. The thermal Hall conductance in a 2D superconductor is well-known to be related to the Berry curvature [19, 20]:

$$\frac{\kappa_{xy}}{T} = -\frac{k_B^2}{2\hbar} \int_{-\infty}^{\infty} dE \frac{E^2}{(k_B T)^2} \sigma(E) f'(E), \quad (5)$$

where $f(E)$ is the Fermi-Dirac function, and

$$\sigma(E) \equiv -\sum_{\mathbf{a}} \int_{E_{\mathbf{k}} < E} \frac{d^2k}{(2\pi)^2} \Omega_{\mathbf{k}}^{\mathbf{a}}. \quad (6)$$

$\Omega_{\mathbf{k}}^{\mathbf{a}} = -2\text{Im}\langle \partial_{k_x} \mathbf{u}_{\mathbf{k}}^{\mathbf{a}} | \partial_{k_y} \mathbf{u}_{\mathbf{k}}^{\mathbf{a}} \rangle$ is the Berry curvature while \mathbf{a} labeling bands of the Bogoliubov-de Gennes (BdG) Hamiltonian below (In this paper we use bold font for quantities related to the superconducting BdG state, to distinguish from the normal state quantities)

$$\mathbf{H}(\mathbf{k}) = \begin{pmatrix} H_0(\mathbf{k}) & \Delta_{\mathbf{k}} \\ \Delta_{\mathbf{k}} & -H_0(\mathbf{k}) \end{pmatrix}. \quad (7)$$

Here the time-reversal transformation is $\psi_{\mathbf{k}} \rightarrow \Lambda K \psi_{\mathbf{k}}$, where K is conjugation and Λ is unitary. And we have used the Nambu basis $\{\psi_{\mathbf{k}}, \Lambda^\dagger \psi_{-\mathbf{k}}^\dagger\}$, ensuring $\Delta_{\mathbf{k}}^\dagger = \Delta_{\mathbf{k}}$.

One can always order the energy eigenvalues of $\mathbf{H}(\mathbf{k})$ into pairs $\pm \mathbf{E}_{1,\mathbf{k}}, \pm \mathbf{E}_{2,\mathbf{k}}, \pm \mathbf{E}_{3,\mathbf{k}} \dots$ with $0 < \mathbf{E}_{1,\mathbf{k}} < \mathbf{E}_{2,\mathbf{k}} < \mathbf{E}_{3,\mathbf{k}} \dots$, and will use $\mathbf{a} = \pm 1, \pm 2, \pm 3 \dots$ to label these bands, i.e., $\mathbf{E}_{-\mathbf{a},\mathbf{k}} = -\mathbf{E}_{\mathbf{a},\mathbf{k}}$. Assuming only intraband pairing is present, we have $\mathbf{E}_{|\mathbf{a}|,\mathbf{k}} = \sqrt{\epsilon_{|\mathbf{a}|,\mathbf{k}}^2 + \Delta_{|\mathbf{a}|,\mathbf{k}}^2}$, where $\epsilon_{a,\mathbf{k}}$ is the normal state band energies ($a = 1, 2, 3 \dots$). Right at a Fermi surface $\epsilon_{1,\mathbf{k}} = 0$, the gap function is $\Delta_{\mathbf{k}} \equiv \Delta_{1,\mathbf{k}}$, and we denote $t \equiv \text{Min}[\epsilon_{b,\mathbf{k}}]$ ($b \neq 1$) as the interband energy scale. We will consider the weak-pairing limit $|\Delta_{\mathbf{k}}| \ll t$.

SATHE is zero without the Josephson supercurrent due to time-reversal symmetry. In the presence of the supercurrent, we calculate the perturbative change of the

Berry curvature $\delta\Omega$ under a $\delta\varphi$. Introducing the projector $\mathbf{P}_a \equiv |u_{\mathbf{k}}^a\rangle\langle u_{\mathbf{k}}^a|$, Berry curvature reads

$$\Omega_{\mathbf{k}}^a \doteq \frac{-\text{Im Tr}[\mathbf{P}_a \partial_{k_x} \mathbf{H} \mathbf{P}_{-a} \partial_{k_y} \mathbf{H} \mathbf{P}_a]}{(\mathbf{E}_a - \mathbf{E}_{-a})^2} - (x \leftrightarrow y). \quad (8)$$

Here and below we specify $\mathbf{a} = \pm 1$: only these low energy states contribute to the leading order $\Delta_{\mathbf{k}}/t$ expansion.

After a small Josephson phase $\delta\varphi$ is turned on, $\mathbf{H}, \mathbf{E}_{\pm a}, \mathbf{P}_{\pm a}$ all receive perturbations in Eq.(8). As shown in the Supplemental Material [18], due to the time-reversal symmetry, it turns out that one only needs to consider the contributions from $\delta\mathbf{P}_{\pm a}$. After some manipulations, under the intraband pairing assumption:

$$\frac{\delta\Omega_{\mathbf{k}}^{\mathbf{a},\text{intra.}}}{\delta\varphi} \doteq \sum_{\mathbf{b} \neq \pm \mathbf{a}} 4\text{Im Tr}[\partial_{k_x} \mathbf{P}_a \partial_{k_y} \mathbf{P}_{-\mathbf{a}} \mathbf{P}_b \partial_{\varphi} \mathbf{P}_a \mathbf{P}_a] - (x \leftrightarrow y) \quad (9)$$

One can show that, to the leading order of $\Delta_{\mathbf{k}}/t$ expansion:

$$\frac{\delta\Omega_{\mathbf{k}}^{\mathbf{a},\text{intra.}}}{\delta\varphi} = -\frac{\Delta_{\mathbf{k}}^2}{4\mathbf{E}_a^3} [v_{x,y} \partial_{k_y} \langle u_{\mathbf{k}}^1 | \hat{L} | u_{\mathbf{k}}^1 \rangle - (x \leftrightarrow y)], \quad (10)$$

where $v_{x,y} \equiv \partial_{k_{x,y}} \epsilon_{1,\mathbf{k}}$ is the normal state Fermi velocity. Note that the Berry curvature change is highly concentrated near the Fermi surface due to the denominator. Plugging Eq.(10) into Eq.(5), after some efforts, the main result Eq.(1) is established.

Interband pairing and nodal superconductivity.— When interband pairing is present, the calculation is more sophisticated. However, the result is simple and well-anticipated. Introducing normal state projectors $P_c \equiv |u_{\mathbf{k}}^c\rangle\langle u_{\mathbf{k}}^c|$, we can define the interband pairing operator using $\Delta_{\mathbf{k}}$ in Eq.(7):

$$\Delta_{\mathbf{k}}^{\text{inter.}} \equiv \sum_{b \neq c} P_b \Delta_{\mathbf{k}} P_c. \quad (11)$$

It can be straightforwardly shown that the effective Hamiltonian in the low energy subspace in the presence of $\delta\varphi$ becomes:

$$\begin{aligned} \mathbf{H}_{\text{eff}} &= \delta\varphi \partial_{\varphi} \epsilon_{1,\mathbf{k}} \boldsymbol{\tau}_0 + \epsilon_{1,\mathbf{k}} \boldsymbol{\tau}_3 + \Delta_{\mathbf{k}} \boldsymbol{\tau}_1 + \delta\varphi G_{\mathbf{k}} \boldsymbol{\tau}_2, \\ G_{\mathbf{k}} &\equiv \frac{-1}{2} \text{Re}[\langle u_{\mathbf{k}}^1 | \Delta_{\mathbf{k}}^{\text{inter.}} \hat{L} | u_{\mathbf{k}}^1 \rangle]. \end{aligned} \quad (12)$$

where $\boldsymbol{\tau}$'s are Pauli matrices in the particle-hole space. Both the first and last terms in \mathbf{H}_{eff} have corrections from $\delta\varphi$, but only the last one changes the Berry curvature. It turns out that, to the leading order of $\Delta_{\mathbf{k}}/t$ expansion, the interband contribution to the Berry curvature can be *faithfully* computed by this simple 2-by-2 effective Hamiltonian (see Supplemental Material [18]). Namely,

$$\frac{\delta\Omega_{\mathbf{k}}^{\mathbf{a},\text{inter.}}}{\delta\varphi} = \frac{-\mathbf{d}_{\mathbf{k}} \cdot (\partial_{k_x} \mathbf{d}_{\mathbf{k}} \times \partial_{k_y} \mathbf{d}_{\mathbf{k}})}{2\mathbf{E}_a^3} \quad (13)$$

where $\mathbf{d}_{\mathbf{k}} \equiv (\Delta_{\mathbf{k}}, G_{\mathbf{k}}, \epsilon_{1,\mathbf{k}})$. Similar to the intraband result Eq.(10), these interband contribution also scales as $1/\Delta$ at the Fermi surface. They may also be represented as Fermi surface integrals in the SATHE response and should be added into Eq.(1), i.e., $\frac{\delta\kappa_{xy}}{\delta\varphi \cdot T} = \frac{\delta\kappa_{xy}^{\text{intra.}}}{\delta\varphi \cdot T} + \frac{\delta\kappa_{xy}^{\text{inter.}}}{\delta\varphi \cdot T}$.

In literature, interband pairing has been discussed in the context of multiband superconductors like MgB_2 and iron pnictides [21, 22]. Although in general its effects cannot be neglected, there are many physical situations in which the interband pairing is expected to be small. Below we discuss two different physical scenarios.

First, let us consider the case that each monolayer of the bilayer-JJ itself is superconducting, as in most bilayer-JJ. Here only the intraband pairing near the Fermi level *within each monolayer* needs to be considered to discuss low energy physics. Namely, $\Delta_{\mathbf{k}}$ in Eq.(7) is diagonal in the *monolayer* band basis. However, these low energy bands will hybridize via T_{\perp} in Eq.(3) and interband pairing for the bilayer system can be generated. Nevertheless, at least for homobilayer systems, when the twisting angle θ is small, this T_{\perp} -induced interlayer pairing is small and proportional to θ . This is because when $\theta = 0$, the pairing matrix in the monolayer band basis is proportional to identity and T_{\perp} block will not induce off-diagonal matrix elements, i.e., interband pairings.

Second, if the monolayers are not superconducting and the pairing mechanism in the bilayer-JJ is intrinsic to the heterostructure, like in TBG, the intraband and interband pairings should be determined self-consistently. For example, for boson-mediated superconductivity, the multiband Eliashberg formulation may be applied, which is characterized by the electron-boson coupling matrix $[\alpha^2(\omega)F(\omega)]_{ab}$, where a, b label bands. Either in the regime that intraband coupling is dominant $[\alpha^2(\omega)F(\omega)]_{a=b} \gg [\alpha^2(\omega)F(\omega)]_{a \neq b}$, or in the regime that the intraband coupling is dominant $[\alpha^2(\omega)F(\omega)]_{a=b} \ll [\alpha^2(\omega)F(\omega)]_{a \neq b}$, it is easy to show that only the intraband pairing is significant [23].

However, there is one situation in which the interband contributions may be dominant: when the superconductivity in the bilayer-JJ is nodal. In this case, the node would develop a mass gap $m = \delta\varphi G_{\mathbf{k}}$ right at the nodal point and a Chern number $C = \pm \frac{1}{2}$ is transferred between the low energy BdG bands per node. When total transferred Chern numbers from all nodes is nonzero, the system becomes a chiral topological superconductor with quantized thermal Hall effect when $k_B T \ll |m|$. Such a supercurrent-driven topological superconductivity has been discussed in the context of twisted cuprate bilayers [24–26] and twisted NbSe_2 heterostructures [27].

Applications to FeSe and cuprates.— To demonstrate SATHE we consider two examples, the nodeless FeSe and the nodal cuprate superconducting thin films. $\Delta_{\mathbf{k}}$ in these 2D superconductors has been well characterized by ARPES measurements due to the large energy scale

of $\Delta_{\mathbf{k}}$ and high- T_c . Note that due to the dimensionless nature of the SATHE response, the supercurrent-induced $\kappa_{xy}(T)$ only depends on $\Delta_{\mathbf{k}}/k_B T$. Therefore, these two examples are also instructive for low- T_c superconductors after rescaling the temperature axis.

We firstly consider a twisted bilayer of FeSe. Monolayer FeSe is reported to host a significant nodeless gap anisotropy of the form $\Delta_{\mathbf{k}} = \Delta_0 + \Delta_2 \cos 2\theta_{\mathbf{k}} + \Delta_4 \cos 4\theta_{\mathbf{k}}$, where $\Delta_0 = 9.9\text{meV}$, $\Delta_2 = -1.4\text{meV}$, and $\Delta_4 = 1.2\text{meV}$ [13]. The C_4 -rotation-related elliptic M -pockets within the two-iron BZ [28–30] can be described by the $\mathbf{k} \cdot \mathbf{p}$ expansion within Fe's $\{3d_{xz}, 3d_{yz}\}$ orbitals [31, 32] that $H_M = (\frac{1}{2m}(k_x^2 + k_y^2) - \mu) + ak_x k_y \tau_z$, where τ_z is Pauli matrix of the orbital space, $\mu = 0.08\text{eV}$, $1/2m = 1.4\text{eV} \cdot \text{\AA}^2$ and $a = 0.6\text{eV} \cdot \text{\AA}^2$. Since all Fermi pockets are near the zone boundary, moiré zone folding effect comes into play for the twisted bilayer FeSe, and Bistritzer-MacDonald model [33] is used to construct the normal state Hamiltonian. For example, to the lowest truncation of the moiré BZ, two hopping processes corresponding to $\delta \mathbf{q}^{t,b} = \pm 2K_M \sin \frac{\theta}{2} \hat{k}_y$ are included for the right M -pocket. We set $T_{\perp}^{d_{xz}^t - d_{xz}^b}(\delta \mathbf{q}^{t,b}) = T_{\perp}^{d_{yz}^t - d_{yz}^b}(\delta \mathbf{q}^{t,b}) \simeq T_{\perp} = 15\text{meV}$ and ignore all interorbital hoppings. After turning on such simple T_{\perp} with a twisting angle $\theta = 11.5^\circ$, the Fermi surfaces reconstruct within the moiré BZ (see Fig.2 (a1) and the Supplemental Material [18] for details).

We secondly consider a twisted bilayer of cuprates [34] with a d -wave gap anisotropy $\Delta_{\mathbf{k}} = \Delta_N \cos 2\theta_{\mathbf{k}}$ [35, 36] and the reported relation $8.5k_B T_c = 2\Delta_N$ [37, 38]. The normal state bilayer Hamiltonian is constructed as following: We take the tight-binding model Eq.(2) in Ref. [39] as the monolayer Hamiltonian, and the interlayer tunneling $T_{\perp}(\mathbf{k})$ is obtained from the detailed orbital-analysis in Ref. [26, 40]: $T_{\perp}(\mathbf{k}) = t_z (\frac{1}{4}(\cos k_x^t - \cos k_y^t)(\cos k_y^b - \cos k_x^b) + a_0)$, with an overall factor t_z and the constant $a_0 = 0.4$ determined from DFT simulations [40]. We set $t_z = 0.025t_0$ with $\theta = 0.6^\circ$ ($t_z = 0.01t_0$ with $\theta = 17.2^\circ$) for illustration of chiral topological superconducting phase in (b1), (b2) (topological trivial phase in (c1), (c2)) of Fig.2 for twisted bilayer cuprates. t_0 is the strength of the leading hoppings within the CuO-plane. Here we neglect the moiré zone folding effect due to the following reasoning: First, based on the two-center approximation [33], far away from the zone boundary the moiré zone folding effect may be neglected. Second, the moiré zone folding effect for the Fermi surfaces near the zone boundary does not modify the Fermi surface topology, leaving the results qualitatively unchanged.

Combining both intraband and interband contribution of the supercurrent-induced Berry curvature Eq.(10) and Eq.(13), the thermal Hall conductance $\kappa_{xy}(T)$ are computed for both examples. The results are given in the right panels of Fig.2. The intraband contribution to the SATHE is found to be dominant for twisted FeSe (a2) and the topological trivial case of twisted cuprates (c2), while

the interband contribution is dominant for the topological nontrivial case of twisted cuprates (b2).

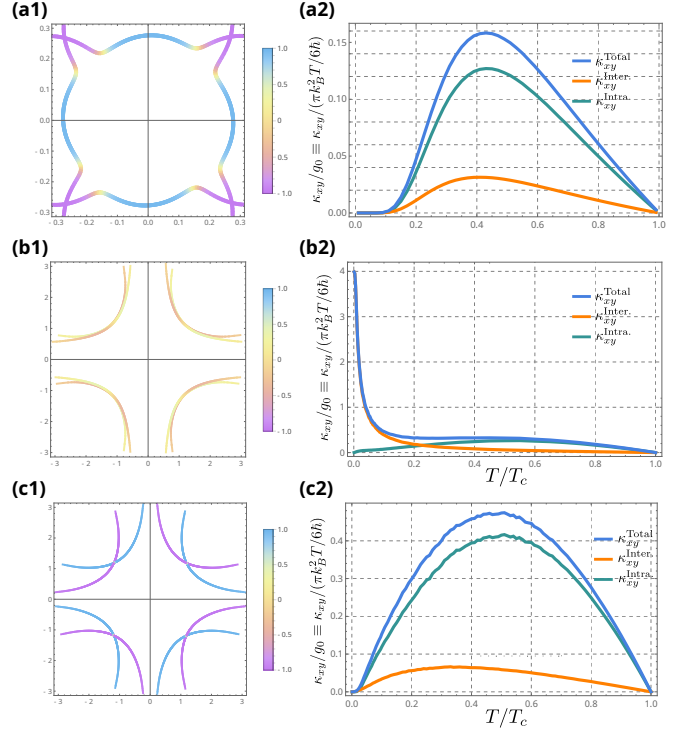


FIG. 2. (a): twisted bilayer FeSe. (b) and (c): the topological non-trivial and trivial phases of twisted bilayer cuprates induced by the supercurrent. The Fermi surfaces are shown on the left panels. For FeSe the moiré zone folding effect plays an important role on the topology of reconstructed Fermi surfaces. The color scheme on each Fermi surface represents the strength of $\langle u_{\mathbf{k}} | \hat{L} | u_{\mathbf{k}} \rangle \in [-1, 1]$. For all three cases, κ_{xy} is induced by a Josephson phase $\varphi = 1.0$ rad, and is computed in unit of the thermal conductance quantum g_0 as a function of temperature, where a simple the mean-field temperature-dependence of $\Delta_{\mathbf{k}}(T) = \Delta_{\mathbf{k}}(T=0)\sqrt{1-T/T_c}$ is implemented. For the topologically nontrivial case (b), gaps $\sim 0.2\text{meV}$ are generated around superconducting nodes due to φ , leading to a Chern number $C = 8$ topological superconductivity, while for the topological trivial case (c) the total Chern number is zero.

Discussion and Conclusion.— In this paper we present the theory for the supercurrent-driven anomalous thermal Hall effect in bilayer Josephson junctions. Different from the conventional thermal Hall effect, in SATHE the time-reversal breaking is provided by the supercurrent in the absence of an external magnetic field. Therefore, SATHE does not involve complications of vortices and is directly coupling to the quasiparticle dynamics in superconductors. Within the BdG mean-field treatment of superconductivity, we showed that SATHE is actually sensitive to the in-plane gap anisotropy in the bilayer-JJ, and serves as a new experimental probe for atomically thin superconducting 2D crystals including twisted bilayer graphene systems, for which experimental probes

have been limited due to the low dimensionality.

Our results can be straightforwardly generalized to multi-layer Josephson junctions. The only modification is that the operator \hat{L} need to be replaced by the generator of the multi-layer gauge transformation.

Recently, motivated by the discovery of novel quantum states in van der Waals materials, the experimental community has made significant progress towards measuring thermal transports in low dimensional systems. For instance, graphene-based Johnson noise thermometry has been developed [41, 42] and used to measure thermal transports in graphene, carbon nanotubes and α -RuCl₃ [43, 44]. Note that the κ_{xy} in the proposed SATHE can reach $\sim 10^{-1}$ of the thermal conductance quantum when the gap anisotropy is significant, e.g., in the FeSe example. We conclude that SATHE can be a sizable effect that may be detectable in the foreseeable future. Particularly for low T_c superconductors, SATHE provides a new probe to detect the gap anisotropy.

Y.R. and X.H. acknowledge the support from National Science Foundation under Grant No. DMR-1712128. J.H.H. was supported by Grant No. NRF-2019R1A6A1A10073079. He also acknowledges financial support from EPiQ Moore theory centers at MIT and Harvard.

-
- [1] Y. Cao, V. Fatemi, S. Fang, K. Watanabe, T. Taniguchi, E. Kaxiras, and P. Jarillo-Herrero, Unconventional superconductivity in magic-angle graphene superlattices, *Nature* **556**, 43 (2018).
- [2] Y. Cao, V. Fatemi, A. Demir, S. Fang, S. L. Tomarken, J. Y. Luo, J. D. Sanchez-Yamagishi, K. Watanabe, T. Taniguchi, E. Kaxiras, *et al.*, Correlated insulator behaviour at half-filling in magic-angle graphene superlattices, *Nature* **556**, 80 (2018).
- [3] K. Krishana, N. Ong, Q. Li, G. Gu, and N. Koshizuka, Plateaus observed in the field profile of thermal conductivity in the superconductor Bi₂Sr₂CaCu₂O₈, *Science* **277**, 83 (1997).
- [4] M. Chiao, R. Hill, C. Lupien, L. Taillefer, P. Lambert, R. Gagnon, and P. Fournier, Low-energy quasiparticles in cuprate superconductors: A quantitative analysis, *Physical Review B* **62**, 3554 (2000).
- [5] M. Sutherland, D. Hawthorn, R. Hill, F. Ronning, S. Wakimoto, H. Zhang, C. Proust, E. Boaknin, C. Lupien, L. Taillefer, *et al.*, Thermal conductivity across the phase diagram of cuprates: Low-energy quasiparticles and doping dependence of the superconducting gap, *Physical Review B* **67**, 174520 (2003).
- [6] A. C. Durst, A. Vishwanath, and P. A. Lee, Weak-field thermal Hall conductivity in the mixed state of d-wave superconductors, *Physical Review Letters* **90**, 187002 (2003).
- [7] Y. Zhang, N. Ong, P. Anderson, D. Bonn, R. Liang, and W. Hardy, Giant enhancement of the thermal Hall conductivity κ_{xy} in the superconductor YBa₂Cu₃O₇, *Physical Review Letters* **86**, 890 (2001).
- [8] V. Cvetkovic and O. Vafek, Berry phases and the intrinsic thermal Hall effect in high-temperature cuprate superconductors, *Nature Communications* **6**, 1 (2015).
- [9] M. Banerjee, M. Heiblum, V. Umansky, D. E. Feldman, Y. Oreg, and A. Stern, Observation of half-integer thermal hall conductance, *Nature* **559**, 205 (2018).
- [10] T. Yokoi, S. Ma, Y. Kasahara, S. Kasahara, T. Shibauchi, N. Kurita, H. Tanaka, J. Nasu, Y. Motome, C. Hickey, *et al.*, Half-integer quantized anomalous thermal hall effect in the kitaev material candidate α -rucl3, *Science* **373**, 568 (2021).
- [11] Z.-X. Shen, D. Dessau, B. Wells, D. King, W. Spicer, A. Arko, D. Marshall, L. Lombardo, A. Kapitulnik, P. Dickinson, *et al.*, Anomalous large gap anisotropy in the a-b plane of Bi₂Sr₂CaCu₂O_{8+ δ} , *Physical Review Letters* **70**, 1553 (1993).
- [12] H. Ding, M. Norman, J. Campuzano, M. Randeria, A. Bellman, T. Yokoya, T. Takahashi, T. Mochiku, and K. Kadowaki, Angle-resolved photoemission spectroscopy study of the superconducting gap anisotropy in Bi₂Sr₂CaCu₂O_{8+ x} , *Physical Review B* **54**, R9678 (1996).
- [13] Y. Zhang, J. Lee, R. Moore, W. Li, M. Yi, M. Hashimoto, D. Lu, T. Devereaux, D.-H. Lee, and Z.-X. Shen, Superconducting gap anisotropy in monolayer fese thin film, *Physical Review Letters* **117**, 117001 (2016).
- [14] T. Hanaguri, Y. Kohsaka, J. Davis, C. Lupien, I. Yamada, M. Azuma, M. Takano, K. Ohishi, M. Ono, and H. Takagi, Quasiparticle interference and superconducting gap in Ca_{2- x} Na _{x} CuO₂Cl₂, *Nature Physics* **3**, 865 (2007).
- [15] P. O. Sprau, A. Kostin, A. Kreisel, A. E. Böhmer, V. Taufour, P. C. Canfield, S. Mukherjee, P. J. Hirschfeld, B. M. Andersen, and J. S. Davis, Discovery of orbital-selective cooper pairing in fese, *Science* **357**, 75 (2017).
- [16] I. Sodemann and L. Fu, Quantum nonlinear Hall effect induced by berry curvature dipole in time-reversal invariant materials, *Physical Review Letters* **115**, 216806 (2015).
- [17] Q. Ma, S.-Y. Xu, H. Shen, D. MacNeill, V. Fatemi, T.-R. Chang, A. M. Mier Valdivia, S. Wu, Z. Du, C.-H. Hsu, *et al.*, Observation of the nonlinear hall effect under time-reversal-symmetric conditions, *Nature* **565**, 337 (2019).
- [18] ee Supplemental Material at [URL_to_be_inserted_by_publisher](#) for detailed derivation on both intraband and interband contribution of SATHE. The explanation on the nodal origin of the interband contribution and the Fermi surface reconstruction of twisted-bilayer FeSe are also discussed.
- [19] T. Qin, Q. Niu, and J. Shi, Energy magnetization and the thermal Hall effect, *Physical Review Letters* **107**, 236601 (2011).
- [20] H. Sumiyoshi and S. Fujimoto, Quantum thermal Hall effect in a time-reversal-symmetry-broken topological superconductor in two dimensions: approach from bulk calculations, *Journal of the Physical Society of Japan* **82**, 023602 (2013).
- [21] A. Vargas-Paredes, A. Shanenko, A. Vagov, M. Milošević, and A. Perali, Crossband versus intraband pairing in superconductors: Signatures and consequences of the interplay, *Physical Review B* **101**, 094516 (2020).
- [22] R. M. Fernandes and J. Schmalian, Competing order and nature of the pairing state in the iron pnictides, *Physical Review B* **82**, 014521 (2010).
- [23] O. V. Dolgov, I. I. Mazin, D. Parker, and A. A.

- Golubov, Interband superconductivity: contrasts between Bardeen-Cooper-Schrieffer and Eliashberg theories, *Physical Review B* **79**, 060502 (2009).
- [24] P. A. Volkov, J. H. Wilson, and J. Pixley, Magic angles and current-induced topology in twisted nodal superconductors, arXiv preprint arXiv:2012.07860 (2020).
- [25] O. Can, T. Tummuru, R. P. Day, I. Elfimov, A. Damascelli, and M. Franz, High-temperature topological superconductivity in twisted double-layer copper oxides, *Nature Physics* **17**, 519 (2021).
- [26] X.-Y. Song, Y.-H. Zhang, and A. Vishwanath, Doping a moiré mott insulator: A t - J model study of twisted cuprates, *Physical Review B* **105**, L201102 (2022).
- [27] X. Hu and Y. Ran, Engineering chiral topological superconductivity in twisted ising superconductors, *Physical Review B* **106**, 125136 (2022).
- [28] V. Brouet, M. F. Jensen, P.-H. Lin, A. Taleb-Ibrahimi, P. Le Fèvre, F. Bertran, C.-H. Lin, W. Ku, A. Forget, and D. Colson, Impact of the two fe unit cell on the electronic structure measured by arpes in iron pnictides, *Physical Review B* **86**, 075123 (2012).
- [29] S. Borisenko, D. Evtushinsky, Z.-H. Liu, I. Morozov, R. Kappenberger, S. Wurmehl, B. Büchner, A. Yaresko, T. Kim, M. Hoesch, *et al.*, Direct observation of spin-orbit coupling in iron-based superconductors, *Nature Physics* **12**, 311 (2016).
- [30] M. Yi, Z. Liu, Y. Zhang, R. Yu, J.-X. Zhu, J. Lee, R. Moore, F. Schmitt, W. Li, S. Riggs, *et al.*, Observation of universal strong orbital-dependent correlation effects in iron chalcogenides, *Nature Communications* **6**, 1 (2015).
- [31] D. Agterberg, T. Shishidou, J. O'Halloran, P. Brydon, and M. Weinert, Resilient nodeless d-wave superconductivity in monolayer fese, *Physical Review Letters* **119**, 267001 (2017).
- [32] Y. Ran, F. Wang, H. Zhai, A. Vishwanath, and D.-H. Lee, Nodal spin density wave and band topology of the feas-based materials, *Physical Review B* **79**, 014505 (2009).
- [33] R. Bistritzer and A. H. MacDonald, Moiré bands in twisted double-layer graphene, *Proceedings of the National Academy of Sciences* **108**, 12233 (2011).
- [34] Note that the currently available cuprate van der Waals materials is Bi2212, which is a bilayer of Cu-O planes. Consequently, twisted *double* bilayer is more experimental relevant at present [45, 46]. Our twisted bilayer model can viewed as a minimal illustration on SATHE for twisted nodal superconductors.
- [35] A. Kanigel, U. Chatterjee, M. Randeria, M. Norman, S. Souma, M. Shi, Z. Li, H. Raffy, and J. Campuzano, Protected nodes and the collapse of fermi arcs in high- T_c cuprate superconductors, *Physical Review Letters* **99**, 157001 (2007).
- [36] T. Kondo, W. Malaeb, Y. Ishida, T. Sasagawa, H. Sakamoto, T. Takeuchi, T. Tohyama, and S. Shin, Point nodes persisting far beyond T_c in Bi2212, *Nature Communications* **6**, 1 (2015).
- [37] C. Kendziora, R. Kelley, and M. Onellion, Superconducting gap anisotropy vs doping level in high- T_c cuprates, *Physical Review Letters* **77**, 727 (1996).
- [38] H. Anzai, A. Ino, M. Arita, H. Namatame, M. Taniguchi, M. Ishikado, K. Fujita, S. Ishida, and S. Uchida, Relation between the nodal and antinodal gap and critical temperature in superconducting Bi2212, *Nature Communications* **4**, 1 (2013).
- [39] M. Eschrig and M. Norman, Effect of the magnetic resonance on the electronic spectra of high- T_c superconductors, *Physical Review B* **67**, 144503 (2003).
- [40] R. Markiewicz, S. Sahrakorpi, M. Lindroos, H. Lin, and A. Bansil, One-band tight-binding model parametrization of the high- T_c cuprates including the effect of k_z dispersion, *Physical Review B* **72**, 054519 (2005).
- [41] K. C. Fong and K. Schwab, Ultrasensitive and wide-bandwidth thermal measurements of graphene at low temperatures, *Physical Review X* **2**, 031006 (2012).
- [42] A. V. Talanov, J. Waissman, T. Taniguchi, K. Watanabe, and P. Kim, High-bandwidth, variable-resistance differential noise thermometry, *Review of Scientific Instruments* **92**, 014904 (2021).
- [43] K. C. Fong, E. E. Wollman, H. Ravi, W. Chen, A. A. Clerk, M. Shaw, H. Leduc, and K. Schwab, Measurement of the electronic thermal conductance channels and heat capacity of graphene at low temperature, *Physical Review X* **3**, 041008 (2013).
- [44] J. Waissman, L. E. Anderson, A. V. Talanov, Z. Yan, Y. J. Shin, D. H. Najafabadi, M. Rezaee, X. Feng, D. G. Nocera, T. Taniguchi, *et al.*, Electronic thermal transport measurement in low-dimensional materials with graphene non-local noise thermometry, *Nature Nanotechnology* **17**, 166 (2022).
- [45] Y. Zhu, M. Liao, Q. Zhang, H.-Y. Xie, F. Meng, Y. Liu, Z. Bai, S. Ji, J. Zhang, K. Jiang, *et al.*, Presence of s-wave pairing in josephson junctions made of twisted ultrathin Bi₂Sr₂CaCu₂O_{8+x} flakes, *Physical Review X* **11**, 031011 (2021).
- [46] S. Zhao, N. Poccia, X. Cui, P. A. Volkov, H. Yoo, R. Engelke, Y. Ronen, R. Zhong, G. Gu, S. Plugge, *et al.*, Emergent interfacial superconductivity between twisted cuprate superconductors, arXiv preprint arXiv:2108.13455 (2021).

Supplemental Material for ‘‘Supercurrent-induced Anomalous Thermal Hall Effect as a New Probe to Superconducting Gap Anisotropy’’

Details on the Derivation of the Main Result

Supercurrent-induced Berry Curvature for Intraband Pairing

Here we provide details of the derivation of the main result Eq.(1) in the main text. Because only $\mathbf{a} = \pm 1$ bands contribute to the low-energy Berry curvature, we will start with Eq.(8) in the main text.

Denoting the c -th eigenstate of $H_0(\mathbf{k})$ as $|u_{\mathbf{k}}^c\rangle: H_0(\mathbf{k})|u_{\mathbf{k}}^c\rangle = \epsilon_{c,\mathbf{k}}|u_{\mathbf{k}}^c\rangle$, and introducing the normal state projector $P_c \equiv |u_{\mathbf{k}}^c\rangle\langle u_{\mathbf{k}}^c|$, we can define the BdG projector into the low energy Hilbert space:

$$\mathbf{P} \equiv P_1 \otimes \tau_0, \quad (14)$$

where τ_0 is the identity Pauli matrix in the particle-hole space. The low-energy BdG Hamiltonian is simply the two-by-two matrix, which perfectly decouples from the high energy Hilbert space if only intraband pairing is present (which we call *intraband pairing assumption* below):

$$\mathbf{PHP} = P_1 \otimes (\epsilon_{1,\mathbf{k}}\tau_3 + \Delta_{\mathbf{k}}\tau_1). \quad (15)$$

Here $\Delta_{\mathbf{k}}$ is chosen to be real due to the time-reversal symmetry. In addition, Projector \mathbf{P} satisfies an important identity with any operator of the following form:

$$\mathbf{A}^\vee \equiv A \otimes \tau_0 \Rightarrow \mathbf{PAP} = \langle u_{\mathbf{k}}^1 | A | u_{\mathbf{k}}^1 \rangle \mathbf{P}, \quad (16)$$

which in turn indicates $\mathbf{P}_{-\mathbf{a}}\mathbf{A}^\vee\mathbf{P}_{\mathbf{a}} = 0$.

After the Josephson-phase $\delta\varphi$ are turned on, $\mathbf{H}, \mathbf{E}_{\pm\mathbf{a}}, \mathbf{P}_{\pm\mathbf{a}}$ all receive perturbations in Eq.(8) in the main text. $\delta\mathbf{H}$ and $\delta\mathbf{E}_{\pm\mathbf{a}}$ do not contribute because $\partial_\varphi\mathbf{H}$ and $\partial_{k_x}\partial_\varphi\mathbf{H}$ both have the form of \mathbf{A}^\vee *under the intraband assumption*. For instance:

$$\partial_\varphi\mathbf{H} = \partial_\varphi H_0(\mathbf{k}) \otimes \tau_0. \quad (17)$$

Thus we are left with the $\delta\mathbf{P}_{\pm\mathbf{a}}$ contribution only:

$$\frac{\delta\Omega^{\mathbf{a}}}{\delta\varphi} \doteq \frac{-\text{Im Tr}[\mathbf{P}_{\mathbf{a}}\partial_{k_x}\mathbf{HP}_{-\mathbf{a}}\partial_{k_y}\mathbf{H}\partial_\varphi\mathbf{P}_{\mathbf{a}}]}{\mathbf{E}_{\mathbf{a}}^2} - (x \leftrightarrow y). \quad (18)$$

Here we used the time-reversal symmetry combined with the particle-hole symmetry, which dictates that the $\delta\mathbf{P}_{-\mathbf{a}}$ contribution and $\delta\mathbf{P}_{\mathbf{a}}$ contribution are identical. After inserting $\mathbf{1} = \sum_{\mathbf{c}}\mathbf{P}_{\mathbf{c}}$ in front of $\partial_\varphi\mathbf{P}_{\mathbf{a}}$, and noting that only terms with $\mathbf{c} \neq \pm\mathbf{a}$ contributes *under the intraband pairing assumption*, the above expression can be rewritten as:

$$\begin{aligned} \frac{\delta\Omega^{\mathbf{a}}}{\delta\varphi} &\doteq \sum_{\mathbf{b} \neq \pm\mathbf{a}} \frac{\text{Im Tr}[\mathbf{P}_{\mathbf{a}}\partial_{k_x}\mathbf{HP}_{-\mathbf{a}}\partial_{k_y}\mathbf{HP}_{\mathbf{b}}\partial_\varphi\mathbf{HP}_{\mathbf{a}}]}{\mathbf{E}_{\mathbf{a}}^2(\mathbf{E}_{\mathbf{b}} - \mathbf{E}_{\mathbf{a}})} - (x \leftrightarrow y) \\ &= \sum_{\mathbf{b} \neq \pm\mathbf{a}} \frac{\text{Im Tr}[\mathbf{P}_{\mathbf{a}}\partial_{k_x}\mathbf{HP}_{-\mathbf{a}}\partial_{k_y}\mathbf{P}_{\mathbf{b}}\partial_\varphi\mathbf{HP}_{\mathbf{a}}]}{\mathbf{E}_{\mathbf{a}}^2(\mathbf{E}_{\mathbf{b}} - \mathbf{E}_{\mathbf{a}})}(\mathbf{E}_{\mathbf{b}} + \mathbf{E}_{\mathbf{a}}) - (x \leftrightarrow y) \\ &= \sum_{\mathbf{b} \neq \pm\mathbf{a}} \frac{2\text{Im Tr}[\mathbf{P}_{\mathbf{a}}\partial_{k_x}\mathbf{HP}_{-\mathbf{a}}\partial_{k_y}\mathbf{P}_{\mathbf{b}}\partial_\varphi\mathbf{HP}_{\mathbf{a}}]}{\mathbf{E}_{\mathbf{a}}(\mathbf{E}_{\mathbf{b}} - \mathbf{E}_{\mathbf{a}})} - (x \leftrightarrow y) \\ &\quad + \sum_{\mathbf{b} \neq \pm\mathbf{a}} \frac{\text{Im Tr}[\mathbf{P}_{\mathbf{a}}\partial_{k_x}\mathbf{HP}_{-\mathbf{a}}\partial_{k_y}\mathbf{P}_{\mathbf{b}}\partial_\varphi\mathbf{HP}_{\mathbf{a}}]}{\mathbf{E}_{\mathbf{a}}^2} - (x \leftrightarrow y). \end{aligned} \quad (19)$$

The term in the last line vanishes *under the intraband pairing assumption*: $\mathbf{P} = \mathbf{P}_1 + \mathbf{P}_{-1}$, $\sum_{\mathbf{b} \neq \pm\mathbf{a}}\partial_{k_y}\mathbf{P}_{\mathbf{b}} = -\partial_{k_y}\mathbf{P}$, and the fact that $\partial_{k_y}\mathbf{P}\partial_\varphi\mathbf{H}$ takes the form of \mathbf{A}^\vee . We therefore arrive at:

$$\frac{\delta\Omega^{\mathbf{a},\text{intra.}}}{\delta\varphi} \doteq \sum_{\mathbf{b} \neq \pm\mathbf{a}} 4\text{Im Tr}[\partial_{k_x}\mathbf{P}_{\mathbf{a}}\partial_{k_y}\mathbf{P}_{-\mathbf{a}}\mathbf{P}_{\mathbf{b}}\partial_\varphi\mathbf{P}_{\mathbf{a}}\mathbf{P}_{\mathbf{a}}] - (x \leftrightarrow y)$$

$$\begin{aligned}
&= \sum_{\mathbf{b} \neq \pm \mathbf{a}} \frac{2\text{Im Tr}[\mathbf{P}_{\mathbf{a}} \partial_{k_x} \mathbf{H} \mathbf{P}_{-\mathbf{a}} \partial_{k_y} \mathbf{H} \mathbf{P}_{\mathbf{b}} \partial_{\varphi} \mathbf{H} \mathbf{P}_{\mathbf{a}}]}{\mathbf{E}_{\mathbf{a}}(\mathbf{E}_{\mathbf{b}} - \mathbf{E}_{\mathbf{a}})(\mathbf{E}_{\mathbf{b}} - \mathbf{E}_{-\mathbf{a}})} - (x \leftrightarrow y) \\
&\doteq \sum_{b \neq 1} \frac{2\text{Im Tr}[\mathbf{P}_{\mathbf{a}} \partial_{k_x} \mathbf{H} \mathbf{P}_{-\mathbf{a}} \partial_{k_y} \mathbf{H} (\mathbf{P}_{\mathbf{b}} + \mathbf{P}_{-\mathbf{b}}) \partial_{\varphi} \mathbf{H} \mathbf{P}_{\mathbf{a}}]}{\mathbf{E}_{\mathbf{a}}(\epsilon_b - \epsilon_1)^2} - (x \leftrightarrow y) \\
&= \sum_{b \neq 1} \frac{2\text{Im Tr}[\mathbf{P}_{\mathbf{a}} \partial_{k_x} \mathbf{H} \mathbf{P}_{-\mathbf{a}} \partial_{k_y} \mathbf{H} \mathbf{P}_{\mathbf{b}} \otimes \tau_0 \partial_{\varphi} \mathbf{H} \mathbf{P}_{\mathbf{a}}]}{\mathbf{E}_{\mathbf{a}}(\epsilon_b - \epsilon_1)^2} - (x \leftrightarrow y) \tag{20}
\end{aligned}$$

Now we are ready to connect with the properties of the normal state. Introducing two-dimensional eigenvectors $|\alpha_{\mathbf{c}}\rangle$ in the particle-hole subspace:

$$|\mathbf{u}_{\mathbf{k}}^{\mathbf{c}}\rangle = |u_{\mathbf{k}}^{\mathbf{c}}\rangle \otimes |\alpha_{\mathbf{c}}\rangle, \tag{21}$$

and noting that

$$\partial_k \mathbf{H} = \partial_{\mathbf{k}} H_0(\mathbf{k}) \otimes \tau_3 + O(\partial_{\mathbf{k}} \Delta_{\mathbf{k}}), \tag{22}$$

together with Eq.(17), one has:

$$\begin{aligned}
\frac{\delta \Omega^{\mathbf{a}, \text{intra.}}}{\delta \varphi} &\doteq \sum_{b \neq 1} \frac{2|\langle \alpha_{\mathbf{a}} | \tau_3 | \alpha_{-\mathbf{a}} \rangle|^2 \text{Im Tr}[P_1 \partial_{k_x} H_0 P_1 \partial_{k_y} H_0 P_b \partial_{\varphi} H_0 P_1]}{\mathbf{E}_{\mathbf{a}}(\epsilon_b - \epsilon_1)^2} - (x \leftrightarrow y) \\
&= \sum_{b \neq 1} \frac{2|\langle \alpha_{\mathbf{a}} | \tau_3 | \alpha_{-\mathbf{a}} \rangle|^2 v_x \text{Im Tr}[P_1 \partial_{k_y} H_0 P_b \partial_{\varphi} H_0 P_1]}{\mathbf{E}_{\mathbf{a}}(\epsilon_b - \epsilon_1)^2} - (x \leftrightarrow y) \\
&= -\frac{v_x |\langle \alpha_{\mathbf{a}} | \tau_3 | \alpha_{-\mathbf{a}} \rangle|^2}{\mathbf{E}_{\mathbf{a}}} \Omega_{k_y, \varphi} - (x \leftrightarrow y) = -\frac{\Delta_{\mathbf{k}}^2}{\mathbf{E}_{\mathbf{a}}^3} v_x \Omega_{k_y, \varphi} - (x \leftrightarrow y), \tag{23}
\end{aligned}$$

where $v_x \equiv \partial_{k_x} \epsilon_{1, \mathbf{k}}$, and $\Omega_{k_y, \varphi} \equiv -2\text{Im}[\langle \partial_{k_y} u_{\mathbf{k}}^1 | \partial_{\varphi} u_{\mathbf{k}}^1 \rangle]$ is the *normal-state* Berry curvature w.r.t. k_y and φ . Using the fact that $|\partial_{\varphi} u_{\mathbf{k}}^1\rangle = \frac{-i}{4} \hat{L} |u_{\mathbf{k}}^1\rangle$, the normal-state Berry curvature $\Omega_{k, \varphi}$ can also be expressed as

$$\Omega_{k, \varphi} = \frac{1}{4} \partial_{\mathbf{k}} \langle u_{\mathbf{k}}^1 | \hat{L} | u_{\mathbf{k}}^1 \rangle, \tag{24}$$

so that Eq.(10) in the main text is obtained.

Fermi Surface Integral

The SATHE can be computed using Eq.(5) and Eq.(6) in the main text. Define

$$\Omega(E) \equiv \sum_{\mathbf{a}} \int \frac{d^2 k}{(2\pi)^2} \Omega_{\mathbf{k}}^{\mathbf{a}} \delta(E - \mathbf{E}_{\mathbf{a}, \mathbf{k}}), \tag{25}$$

we have $\sigma(E) = \sigma(0) - \int_0^E dE' \Omega(E')$. Here $\sigma(0) = 0$ due to the time-reversal symmetry and the nodeless assumption.

Because the change of the Berry curvature is concentrated near the Fermi surface due to the $\mathbf{E}_{\mathbf{a}}$ denominator, and proportional to $1/\Delta_{\mathbf{k}}$ right at the Fermi surface, it is convenient to represent $\Omega(E)$ as a Fermi surface integral as following:

$$\begin{aligned}
\frac{\delta \Omega(E)}{\delta \varphi} &\doteq \sum_{\text{FS}} \frac{1}{(2\pi)^2} \oint_{\text{FS}, \epsilon_{\mathbf{k}} \equiv \pm \sqrt{E^2 - \Delta_{\mathbf{k}}^2}} dk_{\parallel} \frac{|E|}{|\epsilon_{\mathbf{k}}| \hbar |v_F|} \frac{1}{\mathbf{E}_{\mathbf{k}}} \Omega_{\mathbf{k}}^{\text{sign}(E)} \\
&\doteq \sum_{\text{FS}} \frac{-2}{(2\pi)^2} \oint_{\text{FS}} dk_{\parallel} \frac{|E|}{\sqrt{E^2 - \Delta_{\mathbf{k}}^2} \hbar |v_F|} \frac{1}{\mathbf{E}_{\mathbf{k}}^3} (v_x \Omega_{k_y, \varphi} - v_y \Omega_{k_x, \varphi}) \\
&= \text{sign}(E) \sum_{\text{FS}} \frac{-1}{2\pi^2} \oint_{\text{FS}} dk_{\parallel} \frac{\Delta_{\mathbf{k}}^2}{E^2 \sqrt{E^2 - \Delta_{\mathbf{k}}^2} \hbar |v_F|} (v_x \Omega_{k_y, \varphi} - v_y \Omega_{k_x, \varphi})
\end{aligned}$$

$$\begin{aligned}
&= \text{sign}(E) \sum_{\text{FS}} \frac{-\text{sign}(v_F)}{2\pi^2\hbar} \oint_{\text{FS}} d\vec{k}_{\parallel} \cdot (\Omega_{k_x, \varphi}, \Omega_{k_y, \varphi}) \frac{\Delta_{\mathbf{k}}^2}{E^2 \sqrt{E^2 - \Delta_{\mathbf{k}}^2}} \\
&= \text{sign}(E) \sum_{\text{FS}} \frac{-\text{sign}(v_F)}{8\pi^2\hbar} \oint_{\text{FS}} dk_{\parallel} \partial_{k_{\parallel}} \langle u_{\mathbf{k}} | \hat{L} | u_{\mathbf{k}} \rangle \frac{\Delta_{\mathbf{k}}^2}{E^2 \sqrt{E^2 - \Delta_{\mathbf{k}}^2}}.
\end{aligned} \tag{26}$$

Integrating out E in advance, we get

$$\sigma(E) = \sum_{\text{FS}} \frac{\text{sign}(v_F)}{8\pi^2\hbar} \oint_{\text{FS}} dk_{\parallel} \partial_{k_{\parallel}} \langle u_{\mathbf{k}} | \hat{L} | u_{\mathbf{k}} \rangle \frac{\sqrt{E^2 - \Delta_{\mathbf{k}}^2}}{|E|} \Theta(|E| - |\Delta_{\mathbf{k}}|). \tag{27}$$

We finally arrive at the result using Eq.(5) in the main text:

$$\frac{\delta\kappa_{xy}}{\delta\varphi T} = \sum_{\text{FS}} \frac{\text{sign}(v_F) k_B^2}{16\pi^2\hbar} \oint_{\text{FS}} dk_{\parallel} \partial_{k_{\parallel}} \langle u_{\mathbf{k}} | \hat{L} | u_{\mathbf{k}} \rangle \xi \left(\frac{\Delta_{\mathbf{k}}}{T} \right). \tag{28}$$

Supercurrent-induced Berry Curvature for Interband Pairing

When interband pairing is present, additional terms need to be considered. However, one can always perform a small unitary rotation $e^{iS \otimes \tau_2}$ to eliminate the interband pairing:

$$S \equiv \sum_{a \neq b} \frac{P_a \Delta_{\mathbf{k}}^{\text{inter.}} P_b}{\epsilon_{a, \mathbf{k}} + \epsilon_{b, \mathbf{k}}}, \quad S^\dagger = S. \tag{29}$$

Since $\mathbf{H} = H_0 \otimes \tau_3 + (\Delta^{\text{intra.}} + \Delta^{\text{inter.}}) \otimes \tau_1$, we have:

$$\begin{aligned}
e^{iS \otimes \tau_2} \mathbf{H} e^{-iS \otimes \tau_2} &\doteq H_0 \otimes \tau_3 + (\Delta^{\text{intra.}} + \Delta^{\text{inter.}}) \otimes \tau_1 + (i)[S \otimes \tau_2, H_0 \otimes \tau_3] \\
&= H_0 \otimes \tau_3 + (\Delta^{\text{intra.}} + \Delta^{\text{inter.}}) \otimes \tau_1 + (i)(SH_0 + H_0S) \otimes (i)\tau_1 \\
&= H_0 \otimes \tau_3 + (\Delta^{\text{intra.}} + \Delta^{\text{inter.}}) \otimes \tau_1 + (-1)\Delta_{\mathbf{k}}^{\text{inter.}} \otimes \tau_1 = H_0 \otimes \tau_3 + \Delta^{\text{intra.}} \otimes \tau_1
\end{aligned} \tag{30}$$

Denoting the projectors in the presence of interband pairing as $\tilde{\mathbf{P}}_{\mathbf{c}}$, we have $\tilde{\mathbf{P}}_{\mathbf{c}} \doteq e^{-iS \otimes \tau_2} \mathbf{P}_{\mathbf{c}} e^{iS \otimes \tau_2}$. Basically, in all the previous derivations for the intraband case, we only need to replace $\mathbf{P}_{\mathbf{c}}$ by $\tilde{\mathbf{P}}_{\mathbf{c}}$, which corresponds to performing the small unitary transformation for the operators like $\partial_{\varphi} \mathbf{H} \rightarrow e^{iS \otimes \tau_2} \partial_{\varphi} \mathbf{H} e^{-iS \otimes \tau_2}$. In this way $\partial_{\varphi} \mathbf{H}$ has a correction $[iS, \partial_{\varphi} H_0] \otimes \tau_2$ and is no longer $\propto \tau_0$. We can leave all the energies $\mathbf{E}_{\mathbf{c}}$ unchanged since they receive second order contributions from $\Delta^{\text{inter.}}$.

After inspection, to the leading order of Δ/t , one can identify three sources of interband contributions. First, we do need to consider $\delta_{\varphi} \partial_{\mathbf{k}} \mathbf{H}$ in Eq.(8) in the main text. Second, in the first line of Eq.(19), $\mathbf{b} = -\mathbf{a}$ needs to be included. Third, the term in the last line of Eq.(19) is no longer vanishing. We term them as *Part-A, B, C* and compute them one by one below.

Part-A: For the $\delta_{\varphi} \partial_{\mathbf{k}} \mathbf{H}$ contributions,

$$\begin{aligned}
\left. \frac{\delta \Omega_{\mathbf{k}}^{\mathbf{a}}}{\delta \varphi} \right|_A &= \frac{-\text{Im Tr} [\mathbf{P}_{\mathbf{a}} \partial_{k_x} \mathbf{H} \mathbf{P}_{-\mathbf{a}} [iS \otimes \tau_2, \partial_{k_y} \partial_{\varphi} \mathbf{H}] \mathbf{P}_{\mathbf{a}}]}{2\mathbf{E}_{\mathbf{a}}^2} - (x \leftrightarrow y) \\
&= \frac{-\text{Im Tr} [\mathbf{P}_{\mathbf{a}} (\partial_{k_x} H_0 \otimes \tau_3 + \partial_{k_x} \Delta \otimes \tau_1) \mathbf{P}_{-\mathbf{a}} [iS \otimes \tau_2, \partial_{k_y} \partial_{\varphi} H_0 \otimes \tau_0] \mathbf{P}_{\mathbf{a}}]}{2\mathbf{E}_{\mathbf{a}}^2} - (x \leftrightarrow y) \\
&= -\langle u_{\mathbf{k}}^1 | [iS, \partial_{k_y} \partial_{\varphi} H_0] | u_{\mathbf{k}}^1 \rangle \\
&\quad \times \frac{v_x \text{Im} [\langle \alpha_{\mathbf{a}} | \tau_3 | \alpha_{-\mathbf{a}} \rangle \langle \alpha_{-\mathbf{a}} | \tau_2 | \alpha_{\mathbf{a}} \rangle] + \langle u_{\mathbf{k}}^1 | \partial_{k_x} \Delta | u_{\mathbf{k}}^1 \rangle \text{Im} [\langle \alpha_{\mathbf{a}} | \tau_1 | \alpha_{-\mathbf{a}} \rangle \langle \alpha_{-\mathbf{a}} | \tau_2 | \alpha_{\mathbf{a}} \rangle]}{2\mathbf{E}_{\mathbf{a}}^2} - (x \leftrightarrow y).
\end{aligned} \tag{31}$$

Noting a few identities:

$$\begin{aligned}
\tau_2 | \alpha_{-\mathbf{a}} \rangle \langle \alpha_{-\mathbf{a}} | \tau_2 &= | \alpha_{\mathbf{a}} \rangle \langle \alpha_{\mathbf{a}} | \\
\partial_{k_x} \mathbf{E}_{\mathbf{a}} &= \text{Tr} [\mathbf{P}_{\mathbf{a}} (\partial_{k_x} H_0 \otimes \tau_3 + \partial_{k_x} \Delta \otimes \tau_1) \mathbf{P}_{\mathbf{a}}] = v_x \frac{\epsilon_{1, \mathbf{k}}}{\mathbf{E}_{\mathbf{a}}} + \langle u_{\mathbf{k}}^1 | \partial_{k_x} \Delta | u_{\mathbf{k}}^1 \rangle \frac{\Delta_{\mathbf{k}}}{\mathbf{E}_{\mathbf{a}}}
\end{aligned}$$

$$\begin{aligned}
\partial_{k_x} \mathbf{E}_a &= \frac{\Delta_k \partial_{k_x} \Delta_k + \epsilon_{1,k} v_x}{\mathbf{E}_a} \\
&\Rightarrow \langle u_k^1 | \partial_{k_x} \Delta | u_k^1 \rangle = \partial_{k_x} \Delta_k \\
\langle \alpha_a | \tau_1 | \alpha_a \rangle &= \frac{\Delta_k}{\mathbf{E}_a}, \quad \langle \alpha_a | \tau_3 | \alpha_a \rangle = \frac{\epsilon_{1,k}}{\mathbf{E}_a}
\end{aligned} \tag{32}$$

we have:

$$\left. \frac{\delta \Omega_k^a}{\delta \varphi} \right|_A = - \frac{\langle u_k^1 | [iS, \partial_{k_y} \partial_\varphi H_0] | u_k^1 \rangle}{2\mathbf{E}_a^3} (-\Delta_k v_x + \epsilon_{1,k} \partial_{k_x} \Delta_k) - (x \leftrightarrow y) \tag{33}$$

Part-B: This term is:

$$\frac{\text{Im Tr}[\mathbf{P}_a \partial_{k_x} \mathbf{H} \mathbf{P}_{-a} \partial_{k_y} \mathbf{H} \mathbf{P}_{-a} \partial_\varphi \mathbf{H} \mathbf{P}_a]}{\mathbf{E}_a^2 (\mathbf{E}_{-a} - \mathbf{E}_a)} - (x \leftrightarrow y) \tag{34}$$

Note that $\mathbf{P}_{-a} \partial_{k_y} \mathbf{H} \mathbf{P}_{-a} = \partial_{k_y} \mathbf{E}_{-a} \mathbf{P}_{-a}$,

$$\begin{aligned}
\left. \frac{\delta \Omega_k^a}{\delta \varphi} \right|_B &= \frac{\partial_{k_y} \mathbf{E}_a}{2\mathbf{E}_a^3} \text{Im Tr}[\mathbf{P}_a (\partial_{k_x} H_0 \otimes \tau_3 + \partial_{k_x} \Delta \otimes \tau_1) \mathbf{P}_{-a} [iS, \partial_\varphi H_0] \otimes \tau_2 \mathbf{P}_a] - (x \leftrightarrow y) \\
&= \frac{\partial_{k_y} \mathbf{E}_a}{2\mathbf{E}_a^3} \langle u_k^1 | [iS, \partial_\varphi H_0] | u_k^1 \rangle \text{Im Tr}[\mathbf{P}_a (\partial_{k_x} H_0 \otimes \tau_3 + \partial_{k_x} \Delta \otimes \tau_1) \mathbf{P}_{-a} \tau_2 \mathbf{P}_a] - (x \leftrightarrow y) \\
&= \frac{\partial_{k_y} \mathbf{E}_a}{2\mathbf{E}_a^3} \langle u_k^1 | [iS, \partial_\varphi H_0] | u_k^1 \rangle \text{Im Tr}[\mathbf{P}_a (\partial_{k_x} H_0 \otimes \tau_3 + \partial_{k_x} \Delta \otimes \tau_1) \tau_2 \mathbf{P}_a] - (x \leftrightarrow y) \\
&= \frac{\partial_{k_y} \mathbf{E}_a}{2\mathbf{E}_a^3} \langle u_k^1 | [iS, \partial_\varphi H_0] | u_k^1 \rangle (-v_x \langle \alpha_a | \tau_1 | \alpha_a \rangle + \langle u_k^1 | \partial_{k_x} \Delta | u_k^1 \rangle \langle \alpha_a | \tau_3 | \alpha_a \rangle) - (x \leftrightarrow y) \\
&= \frac{\partial_{k_y} \mathbf{E}_a}{2\mathbf{E}_a^4} \langle u_k^1 | [iS, \partial_\varphi H_0] | u_k^1 \rangle (-\Delta_k v_x + \epsilon_{1,k} \partial_{k_x} \Delta_k) - (x \leftrightarrow y) \\
&= \frac{(v_y \epsilon_{1,k} + \Delta_k \partial_{k_y} \Delta_k)}{2\mathbf{E}_a^5} \langle u_k^1 | [iS, \partial_\varphi H_0] | u_k^1 \rangle (-\Delta_k v_x + \epsilon_{1,k} \partial_{k_x} \Delta_k) - (x \leftrightarrow y)
\end{aligned} \tag{35}$$

After $(x \leftrightarrow y)$ antisymmetrization, we get

$$\left. \frac{\delta \Omega_k^a}{\delta \varphi} \right|_B = \frac{-1}{2\mathbf{E}_a^3} \langle u_k^1 | [iS, \partial_\varphi H_0] | u_k^1 \rangle v_x \partial_{k_y} \Delta_k - (x \leftrightarrow y) \tag{36}$$

Part-C: Note that

$$\partial_{k_y} \tilde{\mathbf{P}}_b \doteq \partial_{k_y} [\mathbf{P}_b + [-iS \otimes \tau_2, \mathbf{P}_b]] \doteq e^{-iS \otimes \tau_2} \partial_{k_y} \mathbf{P}_b e^{iS \otimes \tau_2} + [-i \partial_{k_y} S \otimes \tau_2, \mathbf{P}_b] \tag{37}$$

The contribution from the last line of Eq.(19) becomes:

$$\begin{aligned}
\left. \frac{\delta \Omega_k^a}{\delta \varphi} \right|_C &\doteq \frac{-\text{Im Tr}[\mathbf{P}_a \partial_{k_x} \mathbf{H} \mathbf{P}_{-a} \partial_{k_y} \mathbf{P} [iS \otimes \tau_2, \partial_\varphi \mathbf{H}] \mathbf{P}_a + \mathbf{P}_a \partial_{k_x} \mathbf{H} \mathbf{P}_{-a} [-i \partial_{k_y} S \otimes \tau_2, \mathbf{P}] \partial_\varphi \mathbf{H} \mathbf{P}_a]}{\mathbf{E}_a^2} - (x \leftrightarrow y) \\
&= \frac{-1}{\mathbf{E}_a^3} (-\Delta_k v_x + \epsilon_{1,k} \partial_{k_x} \Delta_k) \text{Re Tr}[\partial_{k_y} P_1 [iS, \partial_\varphi H_0] P_1 + P_1 i \partial_{k_y} S \partial_\varphi H_0 P_1] - (x \leftrightarrow y) \\
&= \frac{-1}{2\mathbf{E}_a^3} (-\Delta_k v_x + \epsilon_{1,k} \partial_{k_x} \Delta_k) \text{Re Tr}[2 \partial_{k_y} P_1 [iS, \partial_\varphi H_0] P_1 + P_1 [i \partial_{k_y} S, \partial_\varphi H_0] P_1] - (x \leftrightarrow y)
\end{aligned} \tag{38}$$

Let's add part-A and part-C together.

$$\begin{aligned}
\left. \frac{\delta \Omega_k^a}{\delta \varphi} \right|_{A+C} &= \frac{-1}{2\mathbf{E}_a^3} (-\Delta_k v_x + \epsilon_{1,k} \partial_{k_x} \Delta_k) \partial_{k_y} [\text{Re Tr}[P_1 [iS, \partial_\varphi H_0] P_1]] - (x \leftrightarrow y) \\
&= \frac{-1}{2\mathbf{E}_a^3} (-\Delta_k v_x + \epsilon_{1,k} \partial_{k_x} \Delta_k) \partial_{k_y} \langle u_k^1 | [iS, \partial_\varphi H_0] | u_k^1 \rangle - (x \leftrightarrow y)
\end{aligned} \tag{39}$$

The quantity $\langle u_{\mathbf{k}}^1 | [iS, \partial_\varphi H_0] | u_{\mathbf{k}}^1 \rangle$ here and in part-B can be easily computed, which we denote as $G_{\mathbf{k}}$:

$$\begin{aligned}
G_{\mathbf{k}} &\equiv \langle u_{\mathbf{k}}^1 | [iS, \partial_\varphi H_0] | u_{\mathbf{k}}^1 \rangle = -2\text{Im}[\langle u_{\mathbf{k}}^1 | S \partial_\varphi H_0 | u_{\mathbf{k}}^1 \rangle] = -2 \sum_{b \neq 1} \text{Im}[\langle u_{\mathbf{k}}^1 | S | u_{\mathbf{k}}^b \rangle \langle u_{\mathbf{k}}^b | \partial_\varphi H_0 | u_{\mathbf{k}}^1 \rangle] \\
&= -2 \sum_{b \neq 1} \text{Im} \left[\frac{\langle u_{\mathbf{k}}^1 | \Delta^{\text{inter.}} | u_{\mathbf{k}}^b \rangle \langle u_{\mathbf{k}}^b | \partial_\varphi H_0 | u_{\mathbf{k}}^1 \rangle}{\epsilon_{1,\mathbf{k}} + \epsilon_{b,\mathbf{k}}} \right] \doteq -2 \sum_{b \neq 1} \text{Im} \left[\frac{\langle u_{\mathbf{k}}^1 | \Delta^{\text{inter.}} | u_{\mathbf{k}}^b \rangle \langle u_{\mathbf{k}}^b | \partial_\varphi H_0 | u_{\mathbf{k}}^1 \rangle}{-\epsilon_{1,\mathbf{k}} + \epsilon_{b,\mathbf{k}}} \right] \\
&= 2 \sum_{b \neq 1} \text{Im}[\langle u_{\mathbf{k}}^1 | \Delta^{\text{inter.}} | u_{\mathbf{k}}^b \rangle \langle u_{\mathbf{k}}^b | \partial_\varphi H_0 | u_{\mathbf{k}}^1 \rangle] = 2\text{Im}[\langle u_{\mathbf{k}}^1 | \Delta^{\text{inter.}} | \partial_\varphi H_0 | u_{\mathbf{k}}^1 \rangle] = \frac{-1}{2} \text{Re}[\langle u_{\mathbf{k}}^1 | \Delta^{\text{inter.}} \hat{L} | u_{\mathbf{k}}^1 \rangle] \quad (40)
\end{aligned}$$

Putting together, we finally get

$$\frac{\delta \Omega_{\mathbf{k}}^{\text{a,inter.}}}{\delta \varphi} = \frac{\delta \Omega_{\mathbf{k}}^{\text{a}}}{\delta \varphi} \Big|_{A+B+C} = \frac{-1}{2\mathbf{E}_{\mathbf{a}}^3} (-\Delta_{\mathbf{k}} v_x + \epsilon_{1,\mathbf{k}} \partial_{k_x} \Delta_{\mathbf{k}}) \partial_{k_y} G_{\mathbf{k}} + \frac{-1}{2\mathbf{E}_{\mathbf{a}}^3} G_{\mathbf{k}} v_x \partial_{k_y} \Delta_{\mathbf{k}} - (x \leftrightarrow y) \quad (41)$$

It is also instructive to study the behavior of $\partial_\varphi \mathbf{H}$ in the low energy subspace:

$$\tilde{\mathbf{P}} \partial_\varphi \tilde{\mathbf{H}} \tilde{\mathbf{P}} = \mathbf{P} \partial_\varphi \mathbf{H} \mathbf{P} + \mathbf{P} [iS \otimes \tau_2, \partial_\varphi \mathbf{H}] \mathbf{P} = \langle u_{\mathbf{k}}^1 | \partial_\varphi H_0 | u_{\mathbf{k}}^1 \rangle \mathbf{P} + \langle u_{\mathbf{k}}^1 | [iS, \partial_\varphi H_0] | u_{\mathbf{k}}^1 \rangle \mathbf{P} \tau_2 \mathbf{P} \quad (42)$$

The low energy effective Hamiltonian in the presence of $\delta\varphi$ becomes:

$$\mathbf{H}_{\text{eff}} = \delta\varphi \partial_\varphi \epsilon_{1,\mathbf{k}} \tau_0 + \epsilon_{1,\mathbf{k}} \tau_3 + \Delta_{\mathbf{k}} \tau_1 + \delta\varphi G_{\mathbf{k}} \tau_2 = \delta\varphi \partial_\varphi \epsilon_{1,\mathbf{k}} \tau_0 + \mathbf{d}_{\mathbf{k}} \cdot \vec{\tau}, \quad (43)$$

where we introduced vector $\mathbf{d}_{\mathbf{k}} \equiv (\Delta_{\mathbf{k}}, \delta\varphi G_{\mathbf{k}}, \epsilon_{1,\mathbf{k}})$. We merely showed that the interband contribution can be faithfully computed using this effective 2-by-2 Hamiltonian:

$$\delta \Omega_{\mathbf{k}}^{\text{a,inter.}} = -2\text{Im} \text{Tr}[p_{\mathbf{a}} \partial_{k_x} p_{\mathbf{a}} \partial_{k_y} p_{\mathbf{a}}] = \frac{-d_{\mathbf{k}} \cdot (\partial_{k_x} \mathbf{d}_{\mathbf{k}} \times \partial_{k_y} \mathbf{d}_{\mathbf{k}})}{2\mathbf{a} |\mathbf{d}_{\mathbf{k}}|^3} \doteq \frac{-\mathbf{d}_{\mathbf{k}} \cdot (\partial_{k_x} \mathbf{d}_{\mathbf{k}} \times \partial_{k_y} \mathbf{d}_{\mathbf{k}})}{2\mathbf{E}_{\mathbf{a}}^3} \propto \delta\varphi \quad (44)$$

$p_{\mathbf{a}} = \frac{1}{2}(1 + \mathbf{a} \frac{\mathbf{d}_{\mathbf{k}} \cdot \vec{\tau}}{|\mathbf{d}_{\mathbf{k}}|})$ is the projector in this effective model.

When the superconductivity is nodal, near a node, the effective theory becomes a Dirac equation:

$$\mathbf{H}_{\text{eff}}^{\text{node}} = \delta\varphi \partial_\varphi \epsilon_{1,\mathbf{k}} \tau_0 + \hbar v_F k_{\perp} \tau_3 + \hbar v_{\Delta} k_{\parallel} \tau_1 + m \tau_2, \quad (45)$$

where $\hbar v_{\Delta} = \frac{\partial \Delta_{\mathbf{k}}}{\partial k_{\parallel}}$, and $m = \delta\varphi G_{\mathbf{k}_{\text{node}}}$ is the mass gap generated by the supercurrent. It is easy to show that the nodal contribution to $\sigma(E)$ is

$$\sigma^{\text{node}}(E) = \begin{cases} \frac{C}{2\pi}, & \text{if } -|m| < E < |m|, \\ \frac{C|m|}{2\pi|E|}, & \text{otherwise.} \end{cases} \quad (46)$$

Here $C = \pm \frac{1}{2}$ is the Chern number transferred due to m . Performing the energy integral in Eq.(5) in the main text, in the low temperature limit $k_B T \ll |m|$ one recovers the quantized $\kappa_{xy}^{\text{node}}/T = \frac{k_B^2}{\hbar} \frac{C\pi}{12}$. However, in the high-temperature limit $m \ll k_B T$, we have:

$$\frac{\kappa_{xy}^{\text{node}}}{T} \doteq -\frac{k_B^2}{\hbar} \frac{C|m|}{2\pi k_B T} \int_0^\infty x f'(x) dx = \frac{k_B^2}{\hbar} \frac{C \ln 2}{2\pi} \frac{|m|}{k_B T}. \quad (47)$$

Namely there is a $1/T$ tail in $\frac{\kappa_{xy}}{T}$.

As a final remark, in the absence of $\delta\varphi$, it is easy to show that the Berry curvature is nonsingular near the Fermi surface. Consequently, one does not need to consider the contribution to SATHE from $\partial_\varphi \mathbf{E}_{\mathbf{a}}$ in the leading order of Δ/t expansion.

Fermi Surface Reconstruction for Twisted Bilayer FeSe

The effective $\mathbf{k} \cdot \mathbf{p}$ model in the main text is written in the orbital space of $\{3d_{xz}, 3d_{yz}\}$. Because the dominant hopping processes occur within *the same* orbitals, we can treat each orbital separately, or equivalently go back to

the single-iron Brillouin zone to work with one ellipse on each direction. The right horizontal elliptic M -pocket of monolayer FeSe is simply described with

$$h = -\tilde{\mu} + a(k_x - k_M)^2 + bk_y^2 \quad (48)$$

with $\mu = -0.08\text{eV}$, $a = 1.08\text{eV} \cdot \text{\AA}^2$ and $b = 1.6\text{eV} \cdot \text{\AA}^2$. Denoting the rotated monolayer Hamiltonian as $h_{\pm\theta/2}(\mathbf{k})$, the rotated bilayer Hamiltonian *without* interlayer tunnelings is then simply a two-by-two diagonal matrix $H_{w/o T_{\perp}} = \text{diag}\{h_{\theta/2}(\mathbf{k}), h_{-\theta/2}(\mathbf{k})\}$.

Under small twisting angles, two-center approximation applies [33] and the general tunneling strength between the top/bottom Bloch states $|\psi_{\alpha}^t, \mathbf{k}^t\rangle$ and $|\psi_{\beta}^b, \mathbf{k}^b\rangle$ takes the form of

$$t_{\mathbf{k}^t, \mathbf{k}^b}^{\alpha\beta} \equiv \langle \psi_{\alpha}^t | H | \psi_{\beta}^b \rangle = \frac{1}{V} \sum_{\mathbf{G}^t, \mathbf{G}^b} \delta_{\mathbf{k}^t + \mathbf{G}^t, \mathbf{k}^b + \mathbf{G}^b} \cdot e^{-i\mathbf{G}^b \cdot \boldsymbol{\tau}_{\alpha}^b} \cdot t_{\alpha\beta}(\mathbf{k}^t + \mathbf{G}^t) \cdot e^{i\mathbf{G}^t \cdot \boldsymbol{\tau}_{\beta}^t}, \quad (49)$$

where $\mathbf{G}^{t,b}$ are the reciprocal vector of the top/bottom layer and $\boldsymbol{\tau}_{\alpha}^t$ and $\boldsymbol{\tau}_{\beta}^b$ are the sublattice position of the wannier centers of top/bottom states. Now that only one state is left in the single-iron Brillouin zone, we can simply take $t_{\alpha\beta}(\mathbf{k}^t + \mathbf{G}^t) = \delta_{\alpha\beta} t(\mathbf{k}^t + \mathbf{G}^t)$.

The low-energy form of the interlayer tunnelings can be obtained with the expansion $\mathbf{k}^{t,b} \equiv \mathbf{q}^{t,b} + \mathbf{K}_M^{t,b}$, $|\mathbf{q}^{t,b}| \ll 1$. Assuming that the tunneling function $t(\mathbf{k}^t + \mathbf{G}^t)$ only depends on the norm of its arguments, we can take the approximation that

$$t(\mathbf{k}^t + \mathbf{G}^t) \equiv t(\mathbf{q}^t + \mathbf{K}_M^t + \mathbf{G}^t) \doteq t(|\mathbf{K}_M|).$$

Since $|\mathbf{K}_M| \gg |\mathbf{q}^{t,b}|$, only terms with momentum differences $\mathbf{k}^t + \mathbf{G}^t - \mathbf{k}^b - \mathbf{G}^b \propto \theta$ will be left due to the delta function in Eq.(49). Taking the right M -pocket as an example, up to the lowest-order truncation on the grids of the scattering vectors, only two terms of $\delta\mathbf{q}^t$ and $\delta\mathbf{q}^b$ need to be included, as is seen in Fig.3. Denoting $t(|\mathbf{K}_M|)/V \equiv w$,

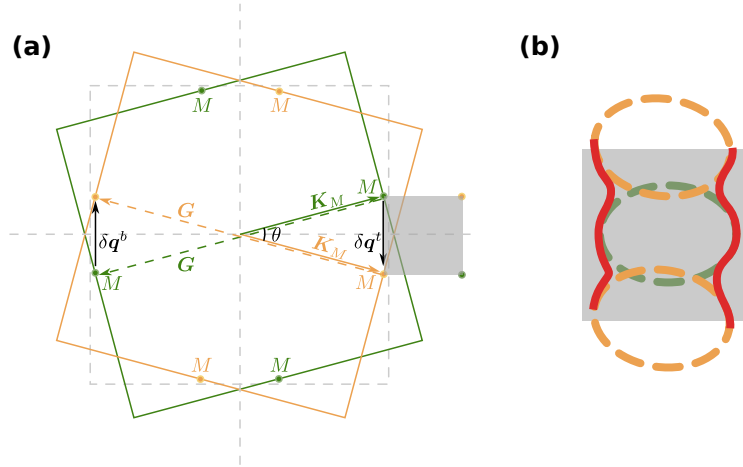


FIG. 3. (a) Rotated top layer (green) and bottom layer (orange). The interference of all different hopping processes capture the spatial variation of interlayer tunnelings, which determines the moiré Brillouin zone (gray square). Up to the lowest truncation on such moiré k -shell, there are just two vertical hopping vectors $\delta\mathbf{q}^t$ and $\delta\mathbf{q}^b$ involved in the reconstruction of the left/right M -pockets (ditto for the top/bottom ones under a C_4 -rotation). (b) Illustration for the moire-pattern-involved Fermi surface reconstruction. Taking the top layer elliptic Fermi surface (green dashed lines) as the reference, both the rotated bottom layer (down orange dashed lines) and the copied M -pockets due to G_x (up orange dashed lines) involve in the reconstruction of the Fermi surfaces (red solid lines).

such truncation gives rise to the minimal moiré Hamiltonian

$$H^{\text{moiré}}(\mathbf{k}) = \begin{pmatrix} h_{\theta/2}(\mathbf{k}) & w & w \\ w & h_{-\theta/2}(\mathbf{k} + \delta\mathbf{q}^t) & 0 \\ w & 0 & h_{-\theta/2}(\mathbf{k} + \delta\mathbf{q}^b) \end{pmatrix}. \quad (50)$$

The moiré pattern-induced Fermi surface reconstruction is then obtained by diagonalization Eq.(50), which recovers the two vertical *open* curves in (a1) of Fig.2 in the main text. The other two horizontal curves comes from the interference of the hopping processes between the up/down M -pockets.